Biochemical Journal (2017) **474** 1705–1725
DOI: 10.1042/BCJ20170125

Research Article

Effect of position-specific single-point mutations and biophysical characterization of amyloidogenic peptide fragments identified from lattice corneal dystrophy patients

Venkatraman Anandalakshmi[1,2,*], Elavazhagan Murugan[1,6,*], Eunice Goh Tze Leng[1], Lim Wei Ting[1], Shyam S. Chaurasia[1,4], Toshio Yamazaki[5], Toshio Nagashima[5], Benjamin Lawrence George[1], Gary Swee Lim Peh[1,6], Konstantin Pervushin[2†], Rajamani Lakshminarayanan[1,6‡] and Jodhbir S. Mehta[1,3,7‡]

[1]Singapore Eye Research Institute, The Academia, 20 College Road, Discovery Tower, Singapore; [2]School of Biological Sciences, Nanyang Technological University, Singapore 637551; [3]Ophthalmology and Visual Sciences Academic Clinical Program, Duke-NUS Graduate Medical School; [4]Department of Veterinary Medicine, Surgery University of Missouri, Columbia, MO, U.S.A.; [5]RIKEN Centre for Life Science Technologies, Kanagawa 230-0045, Japan; [6]Department of Clinical Sciences, Duke-NUS Graduate Medical School, Singapore; and [7]Singapore National Eye Centre, 11 Third Hospital Avenue, Singapore 168751

Correspondence: Jodhbir S. Mehta (jodmehta@gmail.com) or R. Lakshminarayanan (lakshminus@gmail.com) or Konstantin Pervushin (kpervushin@ntu.edu.sg)

Corneal stromal dystrophies are a group of genetic disorders that may be caused by mutations in the transforming growth factor β-induced (*TGFBI*) gene which results in the aggregation and deposition of mutant proteins in various layers of the cornea. The type of amino acid substitution dictates the age of onset, anatomical location of the deposits, morphological features of deposits (amyloid, amorphous powder or a mixture of both forms) and the severity of disease presentation. It has been suggested that abnormal turnover and aberrant proteolytic processing of the mutant proteins result in the accumulation of insoluble protein deposits. Using mass spectrometry, we identified increased abundance of a 32 amino acid-long peptide in the 4th fasciclin-like domain-1 (FAS-1) domain of transforming growth factor β-induced protein (amino acid 611–642) in the amyloid deposits of the patients with lattice corneal dystrophies (LCD). *In vitro* studies demonstrated that the peptide readily formed amyloid fibrils under physiological conditions. Clinically relevant substitution (M619K, N622K, N622H, G623R and H626R) of the truncated peptide resulted in profound changes in the kinetics of amyloid formation, thermal stability of the amyloid fibrils and cytotoxicity of fibrillar aggregates, depending on the position and the type of the amino acid substitution. The results suggest that reduction in the overall net charge, nature and position of cationic residue substitution determines the amyloid aggregation propensity and thermal stability of amyloid fibrils.

*These authors contributed equally to this work.
†Present address: School of Biological Sciences, Nanyang Technological University, Singapore 637551.
‡Present address: The Academia, 20 College Road, Discovery Tower Level 6, Singapore 169856.

Received: 17 February 2017
Revised: 24 March 2017
Accepted: 5 April 2017

Accepted Manuscript online: 5 April 2017
Version of Record published: 9 May 2017

Introduction

Transforming growth factor β-induced (*TGFBI*) corneal stromal dystrophies are a group of genetic disorders associated with the deposition of misfolded protein aggregates in various layers of the cornea. Genetic studies have identified several autosomal dominant mutations in the *TGFBI* gene to be responsible for the protein deposits and the resulting opacification of the cornea that can lead to severe visual impairment [1]. The age of onset for these dystrophies may vary from the first decade of life for severe phenotypes to the eighth or ninth decade for the less severe phenotypes. The nature of the protein deposits and the layer of the cornea affected depend on the type of mutations [2]. Based on slit lamp bio-microscopy and histological examinations, the protein deposits can be classified as amyloidogenic, where the protein deposits appear as thin and long amyloid fibers (lattice corneal

Biochemical Journal (2017) **474** 1705–1725
DOI: 10.1042/BCJ20170125

dystrophy, LCD), non-amyloidogenic (granular corneal dystrophy) where the protein deposits display spherical morphology or a mixed form, where a combination of both fibrils and discrete aggregates are present [3]. *TGFBI*-related corneal dystrophies are mostly limited to Bowman's layer and the stroma. In general, there is a good phenotype–genotype correlation for the *TGFBI*-associated mutations [4]. There are more than 65 different mutations reported to date in the *TGFBI* gene and a majority of them, ∼80%, are located in the 4th FAS-1 domain of the mature protein, making it a mutational hotspot. Despite the sophisticated clearance mechanisms that are required for maintaining corneal transparency, the manner in which the mutant protein aggregates in the cornea remains an enigma [5].

The protein product of *TGFBI* is known as TGFBIp (transforming growth factor β-induced protein), a 683 amino acid-long secretory protein. The protein has four FAS-1 domains, an N-terminal cysteine-rich secretory EMI (Emilin-like domain) and an integrin-binding Arg-Gly-Asp (RGD domain) situated at the C-terminal [6]. TGFBIp is found to be expressed in various normal human tissues, e.g. heart, kidney, liver and skin [7]. In the normal cornea, TGFBIp is expressed abundantly in the epithelium, stroma, Bowman's membrane and endothelium. TGFBIp is shown to interact with various integrins [8,9] and extracellular matrix proteins such as fibronectin, periostin, collagen and proteoglycans. It has been hypothesized that mutations in TGFBIp alter the overall turnover rate of the protein in the cornea [10] with different proteolytic processing mechanism compared to other tissue. Although mutations in *TGFBI* are present throughout the body, protein deposits are found only in the cornea [5], suggesting that, apart from the proteolytic processing and clearance mechanism, there are other intrinsic contributing factors that may lead to cornea-specific protein aggregation and deposition [11–13].

Very few studies have been carried out to understand how the mutant TGFBIp proteins aggregate and form insoluble deposits [14]. Proteomic studies revealed that the mutant TGFBIp protein is proteolytically processed differently in dystrophic cornea than control cornea [15–17]. It has been hypothesized that the proteolytic products with high aggregation propensity may act as fibrillation seeds and trigger an aggregation cascade [17]. The increased abundance of a short peptide fragment in the 4th FAS-1 domain of TGFBIp (Y^{571}HIGDEILVSGGIGALVR^{588}) in amyloid deposits and its ability to accelerate the fibrillation of the mutant protein confirmed the role of aberrant proteolytic fragments in accelerating the fibrillation of larger proteins [18]. The increased abundance of peptide fragments spanning the 4th FAS-1 domain of TGFBIp in the amyloid deposits of dystrophic patients further suggests the importance of this domain in pathophysiology [18].

Sørensen et al. [18] characterized the amyloid fibril forming properties of TGFBIp F^{515}–N^{532} (F^{515}SMLVAAIQSAGLTETLN^{532}) and Y^{571}–R^{588} (Y^{571}HIGDEILVSGGIGALVR^{588}) that were enriched in the amyloid deposits in LCD patients with R124C, V624M and A546D mutations. They further showed that the peptide fragment Y^{571}–R^{588} accelerated the amyloid fibrillation of A546T mutant protein. These results implicated the possible role of amyloidogenic peptide fragments derived from large proteins in the pathology of aggregate formation. Previous studies by our group and the others have suggested that peptide fragments from the 4th FAS 1 domain of TGFBIp form amyloid fibrils under physiological conditions [19,20].

In the present study, we investigated the aggregation propensity of a previously reported 23-residue peptide [20] in the 4th FAS-1 domain (E^{611}PVAEPDIMATNGVVHVITNVLQ^{633}) and its clinically relevant variants which decrease the overall net charge of the peptide. The rationale for choosing this region was based on our proteomics studies that the peptide fragment E^{611}PVAEPDIMATNGVVHVITNVLQPPANRPQER^{642} was enriched in the amyloid deposits of the 4th FAS-1 mutant (R124C and H626R) of TGFBIp [Proteomic analysis of amyloid corneal aggregates from TGFBI-H626R lattice corneal dystrophy patient implicates serine–protease HTRA1 in mutation-specific pathogenesis of TGFBIp — manuscript submitted to *Journal of Proteome Research*]. Interestingly, mutations within this region are associated with amyloidogenic phenotypes [21–25] and majority of the mutations are associated with alteration of overall net charge of the sequence.

Materials and methods

Materials

The $TGFBIp^{611–633}$ wild-type (WT) and mutant synthetic peptides were purchased from Synpeptides (Synpeptide Co. Ltd, Shanghai, China). The purity of peptides was greater than 95% when synthesized (Supplementary Figure S1). Formvar–carbon-coated nickel grids were bought from EMS (Electron Microscopy Sciences, PA, U.S.A.). Chemicals were bought from Sigma–Aldrich Inc. (MO, U.S.A.). Acetonitrile (ACN),

Biochemical Journal (2017) **474** 1705–1725
DOI: 10.1042/BCJ20170125

formic acid and water for mass spectrometric studies were obtained from Sigma–Aldrich (St Louis, MO, U.S.A.). UltraMicro Spin column was bought from The Nest Group (Southborough, MA, U.S.A.).

Spectral counts of tryptic peptides from TGFBIp using LC–MS/MS

Corneal sections were collected from three corneal dystrophy patients with amyloid lattice corneal dystrophy (two patients with H626R mutation and one patient with R124C mutation in the *TGFBI* gene) who were undergoing corneal transplantation at the Singapore National Eye Centre. Written informed consent was obtained from all patients prior to surgery. Ethical approval for the collection of patient corneas was granted by the Singhealth Institutional Review Board. Control tissues ($n = 3$), transplant-grade corneal samples from deceased individuals were obtained from Lion's Eye Institute (Tampa, U.S.A.). The patient corneal sections were stained with Congo red to locate the amyloid fibril deposits. Positive Congo red sections were collected using laser capture microdissection (LCM) and proteins were extracted from the LCM cap. Three normal control corneas without epithelium were dissected into smaller pieces using a sharp scalpel and they were processed to extract corneal stromal proteins. The proteins from patients and controls were digested overnight with 10 μg of trypsin for 16 h at 37 °C and used for mass spectrometry analysis.

LC–MS/MS analysis was performed using a Q Exactive mass spectrometer coupled with the online Dionex Ultimate 3000 RSLC nano-LC system (Thermo Scientific, MA, U.S.A.). Samples were run on a Dionex EASY-spray column (PepMap® C18, 3 μm, 100 Å) using an 120 min gradient of mobile phase A (0.1% FA in 5% ACN) and mobile phase B (0.1% FA in ACN) with a flow rate of 300 nl/min. Separated peptides were passed through an EASY nanospray source with a source voltage of 1.5 kV. A full MS scan was set at 350–1600 m/z with a resolution of 70 000 at m/z 200. The maximum ion accumulation time and dynamic exclusion time were set as 100 ms and 30 s, respectively. The 10 most intense ions detected above a threshold of 1000 counts were selected for higher energy collisional dissociation fragmentation using 28% normalized collision energy with a maximum ion accumulation time of 120 ms. Other parameters used were automatic gain control $1e \times 10^6$ for the full MS scan and $2e \times 10^5$ for the MS2 scan, isolation width of 2 Da for the MS2 scan, and exclusion of single and unassigned charged ions from the MS/MS scan (with the underfill ratio set to 0.1%). Data acquisition was performed using the Xcaliber 2.2 software (Thermo Scientific, U.S.A.).

Data analysis

Raw data were processed using two different approaches to achieve high confidence of label-free quantitation. First, all raw data were converted into the mascot generic format (MGF) using Proteome Discoverer 1.4.1.14 (Thermo Fisher, MA, U.S.A.), and searches were performed using an in-house search engine (Mascot, version 2.4.1; Matrix Science, London, U.K.). The UniProt Knowledgebase (UniProtKB) of human proteins (downloaded on July 25, 2016, including 70 849 sequences and 23 964 784 residues) was used as the search database. The following settings were applied: static modification = carbamidomethyl at cysteine; dynamic modifications = methionine oxidation, asparagine/glutamine deamidation; digestion parameters = full trypsin with maximum two missed cleavages, semi-trypsin with one non-specific cleavage; search parameters = #13C is 2; precursor mass is 10 ppm; fragment mass tolerance is 0.02 Da. Selection of proteins for final analysis was performed using a target-decoy search strategy with a false discovery rate (FDR) of ≤1% considering only those proteins identified with multiple peptides. An additional search was performed using semi-tryptic digestion as the enzyme parameter in order to identify non-tryptic peptide cleavage sites. The emPAI value reported by Mascot and spectral counting was used to perform quantification of proteins and peptides, respectively.

The raw data files were also analyzed using the Proteome Discoverer 1.4 software package. MS/MS spectra were searched against the same UniProt human database using the Mascot search engine with parameters identical with those described above. The peptide-to-spectrum matches were filtered by application of a <1% FDR threshold using Percolator. Only peptides identified with high confidence as assigned by the software were selected for further analysis. The precursor ion area detection node was enabled in order to obtain the area under the curve (AUC, or extracted ion chromatogram/XIC) of the LC elution profiles of the detected peptides. The AUCs of the same peptides obtained from both patient and control samples were used for quantitative analysis to determine the fold changes and extent of enrichment in patient tissues. Peptide/protein lists were exported to Excel and processed using in-house analytical scripts. All statistical calculations were performed using three technical replicates for each sample.

PORTLAND PRESS

Biochemical Journal (2017) 474 1705–1725
DOI: 10.1042/BCJ20170125

Circular dichroism spectroscopy to determine secondary structure of P1 and other mutant peptides

Far UV-circular dichroism (CD) spectra of the peptides were collected using a Jasco J-810 spectropolarimeter (Jasco, Inc., Easton, MD, U.S.A.) and Chirascan-plus (Applied Photophysics, U.K.) using a quartz cuvette with a path length of 0.1 cm (Hellma, Müllheim, Germany/Starna). The TGFBIp$^{611-633}$WT and mutant synthetic peptides were reconstituted in PBS (pH 7.2) to a final concentration of 0.6 mg/ml and their CD spectra were recorded.

For time-dependent conformational transition of the model peptides, the peptides were shaken at 180 rpm at 37°C up to 5 weeks in a shaking incubator. The spectra were recorded from 260 to 190 nm with a step size of 0.1 nm, at a scan rate of 50 nm/min for every 1°C. Initial and final spectra before and after heating and after cooling back to 20°C were recorded. The final spectrum used for plotting was an average of three scans. The CD data were expressed as the mean residual weight ellipticity (deg cm^2 dmol^{-1}). The mean residual weight (MRW) ellipticity ($[\theta]_{MRW}$) was estimated using the following equation:

$$[\theta]_{MRW} = \frac{[\theta]_\lambda \times MRW}{10 \times l \times c}$$

where $[\theta]_\lambda$ is the observed ellipticity, MRW is the mean residual weight and defined as $M/N-1$ where M is the molecular mass and N is the number of amino acid residues, l is the path length of the cuvette and c is the concentration in mg/ml. The data obtained were plotted using the Origin 8.0 software.

To infer if the amyloid fibrils formed by the TGFBIp mutant peptides possess similar or varying thermal properties, we monitored the melting and reassembly of the preformed amyloid fibrils by variable temperature CD spectropolarimetry. To achieve homogeneous amyloid fibril preparations, the peptides were incubated in PBS buffer at 37°C for 5 weeks (10 weeks for P6) until the samples contain a significant abundance of amyloid fibrils. For thermal denaturation experiments, 0.6 mg/ml of the peptide fibrils in PBS (pH 7.2) were heated using the inbuilt Peltier heating system (Applied Photophysics, U.K.). The CD spectra were recorded as described earlier at various time intervals. Variable temperature scanning was done by heating the sample from 20 to 90°C at a rate of 1°C/min.

For studying the effects of ramping rates on the P5 peptide fibrils, the sample was analyzed by heating the fibrils to 90°C at various heating rates (0.5, 1 and 2°C/min).

Thioflavin T assay

The TGFBIp$^{611-633}$WT and mutant synthetic peptides (0.6 mg/ml) were shaken at 180 rpm in a 37°C incubator, and samples were taken at various time points up to 36 h and were treated with 30 μM ThT in PBS buffer (pH 7.2) in a Greiner 96-well flat bottom polystyrol microplate (Greiner, Frickenhausen, Germany). The samples were excited at 445 nm and the resulting emission fluorescence at 485 nm was measured using a microplate reader (Tecan infinite M200 pro, Zanker Road, San Jose, U.S.A.).

Transmission electron microscopy

Transmission electron microscopic images of the peptide fibrils were acquired with a JEOL JEM-1010 transmission electron microscope using Digital Micrograph™ 1.81.78 for GMS 1.8.0 (Gatan, Pleasanton, CA, U.S.A.) at the National University of Singapore Electron Microscopy facility. Aliquots of amyloid fibrils were obtained by shaking 0.6 mg/ml of each of the peptide at 37°C in a shaking incubator. About 500 μl of amyloid fibril samples were withdrawn at different time points and centrifuged gently. The supernatant was removed and 10 μl of amyloid fibril samples were applied onto Formvar-carbon-coated 300-mesh-size nickel grids with bacitracin as the binding agent. Excess samples were blotted off the filter paper and negatively stained with 10% phosphotungstic acid, incubated for 5–10 min and washed with water. The grids were dried and observed at magnifications 8000–50 000× at 80 kV. For thermal denaturation studies on P5-derived fibrils, the fibrils were heated to 90°C and cooled back, centrifuged and examined using transmission electron microscopy (TEM) as described above. The length and mean diameter of the fibrils were calculated by the measurements obtained using the ImageJ software (National Institute of Mental Health, Bethesda, MA, U.S.A.). For enzyme-assisted proteolysis studies, the trypsin-digested fibril samples were examined using TEM as described.

Biochemical Journal (2017) 474 1705–1725
DOI: 10.1042/BCJ20170125

LC–MS/MS analyses

Amyloid fibrils collected from P5 (300 μg) were digested with trypsin (Trypsin : Fibril = 1:25 ratio) for 12 h. The digested mixture was analyzed by LC–MS/MS [Ultimate 3000 nano-LC (Thermo Fisher Scientific/Dionex, Sunnyvale, CA, U.S.A.), coupled with AB SCIEX Triple TOF TM 5600 mass spectrometer] and monitored for the short fragment (E611R623) in the sequence. The peptide mixture was first desalted and pre-concentrated in a trap column (Acclaim PepMap 100 C18, 75 μm × 3 μm, 100 Å from Thermo Fisher Scientific/Dionex) for 3 min at a flow rate of 5 μl/min. After desalting, the system was switched into line with the reversed-phase analytical capillary column (25 cm × 75 μm i.d., Acclaim PepMap RSLC C18, 2 μm, 100 Å, Thermo Fisher Scientific/Dionex, Sunnyvale, CA, U.S.A.). A 35 min gradient was used at 300 nl/min. All data were acquired using the information-dependent acquisition mode with the Analyst TF 1.5.1 software (AB Sciex, U.S.A.). The Protein Pilot software (version 4.01, AB Sciex) was used to analyze the MS/MS data.

Peptide aggregation by one-dimensional solution NMR

For all NMR experiments, peptides P1 to P6 were selectively ^{13}C- and ^{15}N-labeled for amino acids (glycine, alanine, valine and isoleucine) and were purchased from Synpeptides (Synpeptide Co. Ltd, Shanghai, China) with purity greater than 95%. The amino acid residues that were ^{13}C- and ^{15}N-labeled for each peptide are highlighted in blue and given in Table 1.

To follow the aggregation profiles of peptides using one-dimensional (1D) solution NMR, 0.6 mg/ml peptides were dissolved in 1× PBS buffer along with 10% D_2O and 5% 4,4-dimethyl-4-silapentane-1-sulfonic acid (DSS). Samples were transferred to 5 mm NMR tubes and experiments were recorded at 37°C. Aggregation profiles were studied using the 600 MHz Bruker Avance II spectrometer by recording series of 1D NMR spectra. Spectra were collected every 30 min until a clear drop in amide peak intensity was observed in the 1D NMR spectra that served as an indirect readout of aggregation. The NMR data were processed using TopSpin 2.0 (www.bruker-biospin.com) and analyzed using CARA (cara.nmr.ch).

1D NMR intensities between 6.8 and 8.8 ppm for each time point for each peptide were obtained by using the integral function of the Topspin software and normalized to the integral values of the internal standard, DSS. The normalized intensity values were fit using a single-phase decay exponential function. The aggregation rate (K) values for each of the peptides were tabulated.

Packing of fibrils in the rotor for solid-state NMR

About 6 mg of ^{13}C- and ^{15}N-labeled peptides were dissolved in PBS to attain a final concentration of 0.6 mg/ml. The peptides were incubated at 37°C in a shaking incubator in PBS buffer for amyloid fibril formation. The fibrils were collected after 5 weeks. The presence of amyloid fibrils was confirmed by TEM. The fibrils were spun gently and the pellet was collected and sent to RIKEN Institute for solid-state NMR experiments. The pellet sample was filled into the NMR sample rotor by centrifugation in a swing rotor and using a pipetteman tip as a funnel.

Table 1 Peptide sequence of the TGFBIp-4th FAS-1 domain (amino acids 611–633) WT and various disease-associated mutants

The underlined residues are labeled with ^{13}C and ^{15}N isotopes. The total number of amino acids labeled for each residue is also tabulated.

Peptide	Sequence	Number of amino acids ^{13}C-, ^{15}N-labeled	Reference in this manuscript
TGFβIp$^{611–633}$WT	EPVAEPDIMATNGVVHVITNVLQ	10	P1
TGFβIp$^{611–633}$M619K	EPVAEPDIKATNGVVHVITNVLQ	10	P2
TGFβIp$^{611–633}$N622H	EPVAEPDIMATHGVVHVITNVLQ	10	P3
TGFβIp$^{611–633}$N622K	EPVAEPDIMATKGVVHVITNVLQ	10	P4
TGFβIp$^{611–633}$G623R	EPVAEPDIMATNRVVHVITNVLQ	9	P5
TGFβIp$^{611–633}$H626R	EPVAEPDIMATNGVVRVITNVLQ	10	P6

PORTLAND PRESS

Biochemical Journal (2017) 474 1705–1725
DOI: 10.1042/BCJ20170125

Solid-state NMR for the amyloid fibrils

1D and two-dimensional (2D) ^{15}N–^{13}C, correlation experiments were performed on a 700 MHz Bruker (Bruker BioSpin GmbH, Rheinstetten, Germany) Avance III spectrometer with a magic-angle spinning (MAS) rate of 15.75 kHz. Cross-polarization magic-angle spinning (CP-MAS) ^{13}C SS NMR experiments were performed at 25°C. 2D ^{13}C–^{13}C dipolar-assisted rotational resonance (DARR) experiments for the P5 and P1 peptides were performed at 25 and 10°C, with a mixing time of 20, 60, 200 and 600 ms. The spectral width (f2 and f1) was set to 270 ppm and center (f2 and f1) was 97.7 ppm. The number of time domain (TD) data points along f2 and f1 dimensions were 1024 and 768, respectively. The recycling delay was set to 1.5 s with 64 scans. For the NCO and NCA experiments, the spectral width (f2 and f1) was set to 270 and 74 ppm and the center (f2 and f1) was 97.7 and 115 ppm, respectively. The numbers of TD data points along f2 and f1 dimensions were 1024 and 96, respectively. The recycling delay was set to 2 s with 384 scans. For all ^{13}C and ^{15}N experiments, chemical shifts were calibrated from the gyromagnetic ratio based on the H_2O signal. The data were processed using TopSpin 2.0 (www.bruker-biospin.com) and analyzed using CARA (cara.nmr.ch).

Cytotoxicity of amyloid fibrils on cultured human corneal fibroblast cells by xCELLigence

The xCELLigence system (ACEA, San Diego, CA, U.S.A.) was used to investigate the effects of the peptide fibrils of TGFBIp on cultured human corneal fibroblast (HCSF) proliferation and cell death. The E-plate 96 is incorporated with sensor arrays at the bottom of each well, which detects and translates cell attachment in the form of electronic impedance. A parameter termed cell index is derived which corresponds to the relative density and adherence strength of cells in each well. HCSF cells were seeded 7000 cells per well on an E-plate 96, in fibroblast media (DMEM with 10% FBS). The cells were allowed to attach onto the E-plate until the impedance curves reached a plateau. The matured fibrils were formed from 0.6 mg/ml monomeric peptides dissolved in PBS and shaken at 37°C at 180 rpm for 4 weeks. These peptide fibrils were centrifuged and diluted in culture media and treated with the cells. Culture was maintained for 48 h in the xCELLigence real-time cell analysis (RTCA) SP Station, placed in an incubator at 37°C with 5% CO_2. There was no change in media during the 48 hour time period to prevent any fluctuations in the impedance values caused by removing the plate from the RTCA system.

Results

Identification of C-terminal peptide fragments in the amyloid deposits of H626R and R124C mutant

The amyloid deposits from patients' cornea were isolated by LCM and digested with trypsin (a detailed protocol is provided in Materials and Methods). To identify the proteolytic fragments that form the core regions of the amyloid fibrils, we analyzed the total percentage of peptide spectra derived after tryptic digestion of mutant TGFBIp and compared with the fragments present in control TGFBIp. The results of the combined spectral counts of peptides from the three patients and control TGFBIp (Figure 1) show that peptides G^{511}DNRFSMLVAAIQSAGLTETLNR^{533}, Y^{571}HIGDEILVSGGIGALVR^{588}, E^{611}PVAEPDIMATNGVVHVITNVLQPPANRPQER^{642}, L^{497}TPPMGTVMDVLKGDNRFSMLVAAIQS AGLTETLNR^{533}, A^{350}IISNKDILATNGVIHYIDELLIPDS AK^{377}, I^{296}LGDPEALRDLLNNHILK^{313} and H^{187}GMTLTSMYQNSNIQIHHYPNGIVTVNCAR^{216}were significantly enriched in the dystrophic cornea but were absent from the control samples. We next assessed if the peptide fragments contained the altered amino acid residues in the deposits isolated from individual dystrophic patients. In R124C amyloid deposits, we were able to identify two mutant peptides, G^{96}–K^{127} (G^{96}CPAALPLS NLYETLGVVGSTTTQLYTDCTEK^{127}) and V^{91}–K^{127} (V^{91}PGEKGCPAALPLSNLYETLGVVGSTTTQLYT DCTEK^{127}), which carry the cysteine residue. In one of the amyloid deposits collected from H626R patient, we could detect the presence of two peptide fragments, N^{603}–R^{626} (N^{603}NVVSVNKEPVAEPDIMATNGVVR^{626}) and E^{611}–R^{626} (E^{611}PVAEPDIMATNGVVR^{626}), with the altered amino acid sequence.

The change in tryptic peptide profiles between the patient samples and normal control samples may be due to the fact that, in a normal WT protein, the protein is well folded and the hydrophobic residues are not exposed, whereas in the mutant protein, the mutations may cause the proteins to mis/unfold, thus exposing the hydrophobic residues. The hydrophobic residues serve as substrates for various proteolytic enzymes, which result in shorter peptides. The change in the protein folding between the WT and mutant thus produces a

Biochemical Journal (2017) **474** 1705–1725
DOI: 10.1042/BCJ20170125

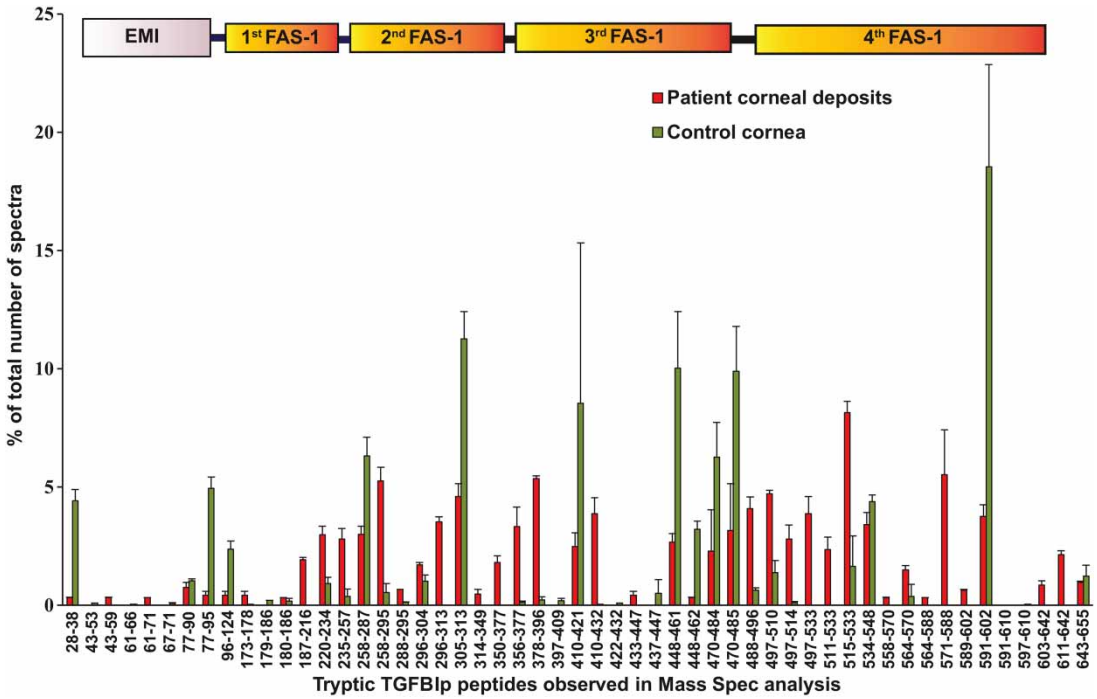

Figure 1. Identification of C-terminal peptide fragments in the amyloid deposits of H626R and R124C mutant.
The spectra show relative abundance of peptides that are highly enriched in the amyloid corneal deposits from corneal dystrophy patients compared with the healthy control cornea. Most peptides enriched in the dystrophy patients are located in the 4th FAS-1 domain, which harbors >80% of all clinically reported mutations.

difference in the accessibility of the proteolytic enzyme action, and hence the peptide generation pattern varies between the WT and mutant proteins.

Cumulative analysis of the mass spectrometric data from three dystrophic patients suggests that, in addition to the previously reported amyloidogenic peptide fragments G^{511}DNRFSMLVAAIQSAGLTETLNR^{533} and Y^{571}-HIGDEILVSGGIGALVR^{588}, the C-terminal fragment E^{611}–R^{642} (E^{611}PVAEPDIMATNGVVHVITNVLQPPAN-RPQER^{642}) was also enriched significantly in the amyloid deposits. This region is clinically important as more than 16 different mutations have been reported and many of them alter the overall net charge of the protein, which leads to the formation of amyloid deposits in the cornea. We recently reported a 23-residue peptide from this region (E^{611}PVAEPDIMATNGVVHVITNVLQ^{633}) that forms amyloid fibrils under physiological conditions [26,27]. Thus, we synthesized five different peptides from clinically significant mutations for the present study (Table 2).

Table 2 Peptide sequence of the TGFBIp-4th FAS-1 domain (amino acids 611–633) WT and various disease-associated mutants
The net charge of each peptide is also tabulated.

Peptide	Sequence	Net charge	Reference in this manuscript
TGFβIp$^{611-633}$WT	EPVAEPDIMATNGVVHVITNVLQ	–3	P1
TGFβIp$^{611-633}$M619K	EPVAEPDI**K**ATNGVVHVITNVLQ	–2	P2
TGFβIp$^{611-633}$N622H	EPVAEPDIMAT**H**GVVHVITNVLQ	–3	P3
TGFβIp$^{611-633}$N622K	EPVAEPDIMAT**K**GVVHVITNVLQ	–2	P4
TGFβIp$^{611-633}$G623R	EPVAEPDIMATN**R**VVHVITNVLQ	–2	P5
TGFβIp$^{611-633}$H626R	EPVAEPDIMATNGVV**R**VITNVLQ	–2	P6

Bold indicates the type of amino acid change (cationic or anionic substitution).

Biochemical Journal (2017) 474 1705–1725
DOI: 10.1042/BCJ20170125

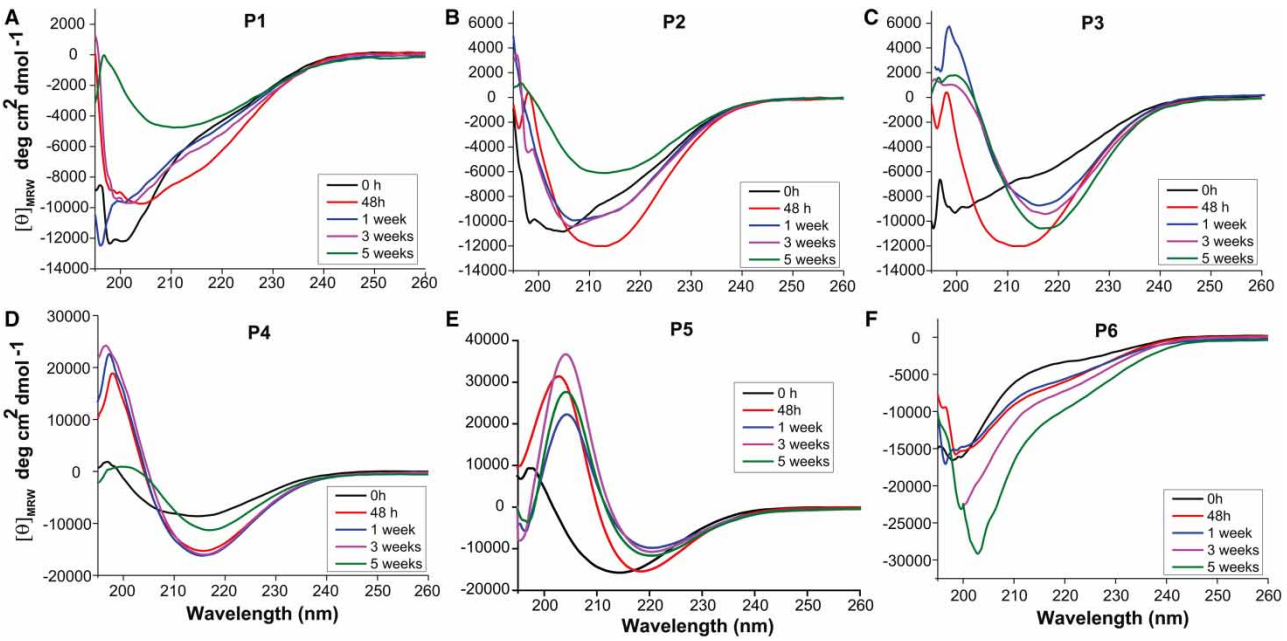

Figure 2. CD spectra of TGFBIp$^{611–633}$WT (P1) and mutant synthetic peptides (P2–P6) in PBS at 37°C were recorded at various time points.
(**A–F**) The results show that TGFBIp$^{611–633}$WT took about 5 weeks to be converted into a β-sheet structure, typical for amyloid fibrils from a random coil configuration. P3, P4 and P5 peptides showed β-sheet transitions as early as week 1. P6 peptide did not show a significant change in the secondary structure even after 8 weeks of monitoring.

Secondary structural analysis and time-dependent conformational transition in model peptides

It has been shown that the conversion from random coil or α-helix into β-sheet conformation is a hallmark of amyloid fibril formation [28,29]. It has been reported that, for β-structured amyloid fibrils, the amplitude of the maximum ∼195–200 nm increased tremendously, higher than the native β-structured protein [30,31]. Therefore, the effect of cationic amino acid substitution on conformational properties of the peptides was investigated by CD spectropolarimetry. We studied the temporal changes in secondary structure of P1–P6 in PBS at 37°C (Figure 2). Figure 2A–F displays temporal changes in the secondary structure of the peptides over a period of 5 weeks. At time 0, P1 (Figure 2A) showed an initial minimum ∼200 nm, typical of an unfolded peptide in equilibrium with a β-sheet structure [28,29,31] and with increase in incubation time, the negative minimum shifts from ∼195–200 nm at 0 h to 210–212 nm at 5 weeks.

All the other mutant peptides, except P6, displayed substantial changes in the secondary structure at time 0 and faster ability to form β-structured assembly as the time progressed when compared with P1 peptide. P2 (Figure 2B) and P3 (Figure 2C) displayed a minimum ∼200 nm and a broad shoulder around n–π* region. A relatively rapid progression was observed for P2 as the β-sheet structures could be seen as early as at 48 h of incubation. The final conformation of P2 appeared to consist of a mixture of secondary structures, as the peptide displayed a broad minimum spanning the region 210–220 nm, indicating the possibility of mixed populations of amyloid oligomers/fibrils. Similar to P2, a rapid conversion into β-structure was apparent for P3 within 48 h. For P4 (Figure 2D), a broad minimum between 205–220 nm and a weak positive peak ∼198 nm was observed, indicating the presence of an ordered secondary structure at time 0 [28,29]. P4 showed a significant increase in the amplitude of the maximum ∼198 nm and the minimum ∼218 nm with an increase in incubation time. CD spectra of P5 (Figure 2E) indicated the presence of an intense minimum ∼218 nm and a strong maximum ∼198 nm, which are characteristics of β-sheet structure at time 0 [28,29]. With increase in time, P5 showed a red shift in both minima and maxima, and the amplitude of π–π* maximum was increased by more than four times the peak intensity at zero time. For P6, the secondary structure was similar to P1 with an intense minimum ∼200 nm (Figure 2F). With increase in time, P6 did not show a transition into β-structured assembly even after 8 weeks of incubation. Thus, substitution of positively charged residues in the

Biochemical Journal (2017) **474** 1705–1725
DOI: 10.1042/BCJ20170125

model peptide had variable effects on the secondary structure and conversion into β-structured assembly, depending on the position and nature of the amino acid substitution.

Aggregation propensity of the amyloid-forming peptides

To analyze the effect of amino acid substitution on the kinetics of amyloid formation, we determined the temporal changes in fluorescence intensity of amyloid-binding dye Thioflavin T (ThT), incubated with the peptides [32–34]. Figure 3 shows the time-dependent changes in the ThT fluorescence intensity. With increase in time, all the mutant peptides (P2–P6) showed a progressive increase in the ThT fluorescence intensity without any lag phase, indicating the presence or formation of amyloid fibrils (Table 3). Peptides P2, P3 and P5 displayed higher k_{agg} and lower $t_{½}$ values, whereas P4 showed similar values when compared with P1. Among all the peptides, P6 displayed the lowest k_{agg} and the highest $t_{½}$, confirming the CD results.

To gain insights into conformational transitions during the early stages, we used 1D proton NMR (Supplementary Figure S2). 1D NMR spectra was recorded at several time points with conditions similar to the ThT experiment. For all the peptides, there was a clear decrease in peak intensity (or broadening of peaks)

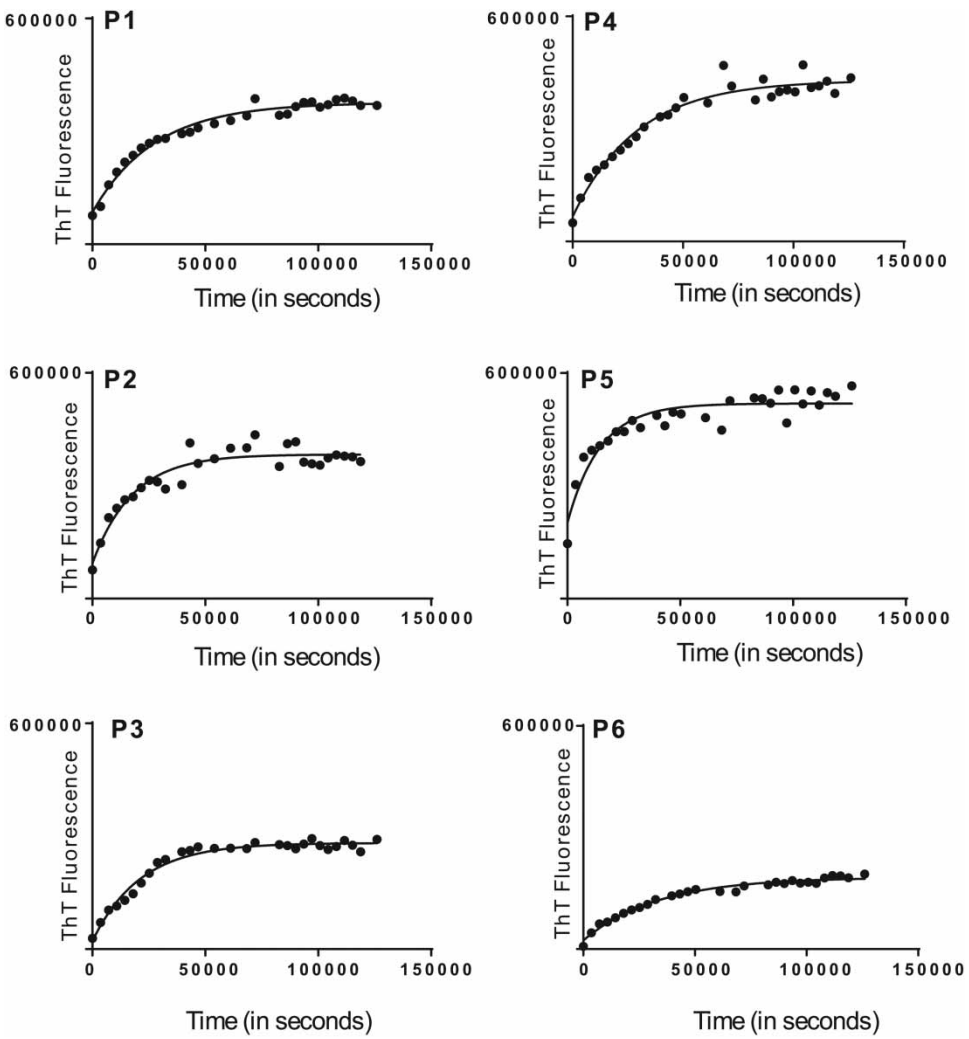

Figure 3. Aggregation kinetics of TGFBIp611–633WT (P1) and mutant peptides (P2–P6) probed by ThT fluorescence.
Aggregation kinetics of TGFBIp$^{611–633}$WT (P1) and mutant peptides (P2–P6) probed by ThT fluorescence. Fluorescence intensity is plotted along the *Y*-axis against the observed time in seconds along the *X*-axis. All the mutant peptides show an increased propensity to form amyloid fibrils compared with the TGFBIp$^{611–633}$WT peptide. ThT intensity data from two independent experiments were averaged for the determination of kinetic parameters.

Biochemical Journal (2017) 474 1705–1725
DOI: 10.1042/BCJ20170125

Table 3 Aggregation rate (k_{agg}) and half-life ($t_{½}$) calculation for the synthetic peptides (P1–P6) to reach half-maximal intensity to form amyloid fibrils based on the observed ThT fluorescence intensity, and aggregation rate (k) calculation for the synthetic peptides (P1–P6) to reach half-maximal intensity to form amyloid fibrils based on normalized intensities calculated from 1D NMR analysis

Peptides	k_{agg}, s^{-1} (ThT assays)	$t_{½}$, h (ThT assays)	Rate constant (K), s^{-1} by 1D NMR
P1	$3.6 \pm 0.3 \times 10^{-5}$	5.3 ± 0.9	–
P2	$5.7 \pm 0.8 \times 10^{-5}$	3.5 ± 1.2	6.94×10^{-5}
P3	$4.7 \pm 0.35 \times 10^{-5}$	4.1 ± 0.6	4.47×10^{-5}
P4	$3.4 \pm 0.38 \times 10^{-5}$	5.9 ± 1.4	3.42×10^{-5}
P5	$6.9 \pm 1.0 \times 10^{-5}$	3.0 ± 1.0	–
P6	$3.0 \pm 0.24 \times 10^{-5}$	6.5 ± 1.1	2.16×10^{-5}

around the amide and aromatic region of the spectra. The decrease in peak intensity or the broadening of the peak is due to the formation of larger molecules, possibly higher order oligomers, that is difficult to be detected by the NMR timescale. This was used as a surrogate to monitor the aggregation process (Supplementary Figure S2A–F). P1 took more than 24 h to aggregate, whereas the P2 peptide aggregated in less than 4 h. For the P3 peptide, a clear decrease in amide peak intensity and peak broadening were also observed in ∼5 h. The P4 peptide aggregated ∼6 h and the P6 peptide aggregated ∼12 h. The P5 peptide was the fastest to aggregate and tended to form oligomers as soon as the peptide was dissolved in the buffer. The amide peaks were not traceable even at time 0. The broadening of 1 D NMR peak intensity, due to formation of oligomer, was plotted against time to obtain the rate constant (K) of aggregation. For each of the time points, the integral values between 6.5 and 8.5 ppm, which showed a maximum change in peak intensity upon aggregation, were collected and normalized with the internal control DSS. The integral values at each time point were used to fit a single-phase decay curve (Figure 4) and the rate constant (K) values were summarized as in Table 2. We could not obtain rate constant (K) values for peptides P1 and P5 as there were not enough points for curve fit. Among the four peptides which could be used for curve-fit analysis, peptide P2 was the fastest to aggregate and peptide P6 was the slowest to form amyloid fibrils. The absence of a lag phase in both ThT and 1D NMR experiments suggests that the aggregation process is spontaneous with the formation of larger oligomers or fibrillar species within a short period of time. Overall, these results are in agreement with the kinetics of aggregation determined by ThT assays. The experiments support the fact that P5 has the fastest rate of aggregation while P1 and P6 peptides displayed slowest rates of aggregation.

Morphology of the amyloid fibrils by TEM

The morphology of amyloid fibrils formed by various peptides was examined by TEM. Upon visual examination, gel-like deposition on the inner walls of the falcon tubes at the rims of the liquid surface with varying levels of transparency and translucency were observed from week 2 onwards. While P3 and P4 displayed nearly transparent deposition, P5 showed more translucent deposition along the inner walls of the tube. The results showed that while all the peptides formed long unbranched fibrils as early as at 2 weeks of incubation, there were differences observed in their morphology, densities, stacking and distribution during the early stages (Figure 5). Images of fibrils formed after 4 days were examined to study the oligomeric, proto-fibrillar or prefibrillar structure and morphologies. It was clear that the oligomers and the protofibrils of the different mutants displayed different morphologies, lengths and diameters. For P1, a mixed population of fibrils and oligomers were observed during early stages. At the end of 2 weeks, clear fibrillation was observed and the oligomeric species were completely absent, indicating partial or complete conversion into amyloid fibrils (Figure 5A). Most of the fibrils of P1 were thin and short in length with a few fibrils extending up to 1–1.2 μm. For P2, more matured fibrils of shorter lengths (100–200 nm) and stacks could be seen during early stages (at 4 days), which then converted into long (1–1.4 μm) unbranched fibrillar assembly after 2 weeks (Figure 5B). For P3, P4 and P5, higher amounts of matured fibrils could be seen in 4 days, with P5 showing the highest abundance of matured fibrils among the three peptides followed by P3 (Figure 5C–E), in accordance with the kinetics of aggregation. All the three peptides showed long fibrillar (2–4 μm) assembly after 2 weeks of incubation. P6,

Biochemical Journal (2017) **474** 1705–1725
DOI: 10.1042/BCJ20170125

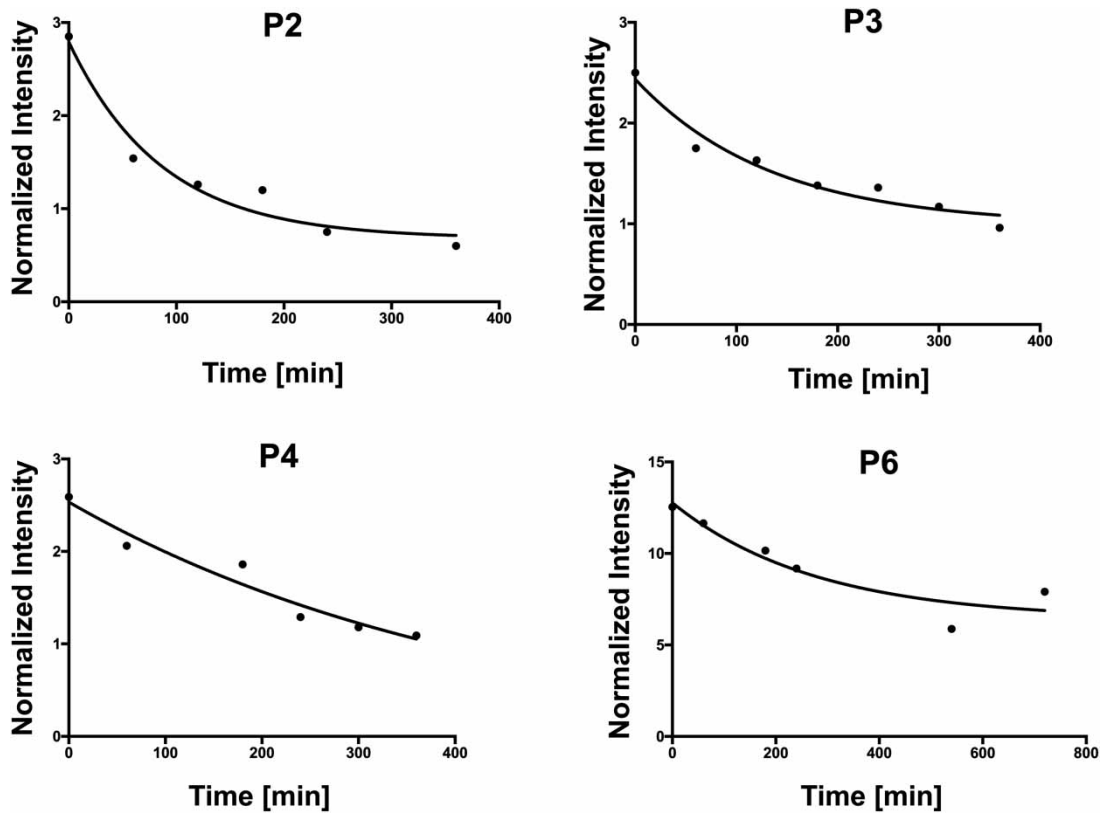

Figure 4. Aggregation kinetics of WT and mutant peptides by 1D NMR.

The normalized intensities of peptide aggregation profiles obtained from 1D NMR at various time points for each of the peptides were fit to a single-phase decay exponential function and the resulting aggregation constant (*K*) values were calculated. Out of the four peptides studied, peptide P2 was the fastest to aggregate and P6 was the slowest to form amyloid fibrils. This result is in agreement with the ThT kinetics.

however, displayed similar morphological features as those of P2, showing a mixed population of oligomers and truncated amyloid fibrils in 4 days, which then formed long amyloid fibrils with increase in incubation time up to 2 weeks (Figure 5F). Estimation of diameters of matured fibrils formed by the peptides did not show any significant differences among the various fibrillar assemblies. These results indicated that despite the changes in kinetics of aggregation and nature of amino acid substitution, all the matured fibrils displayed nearly identical morphologies and diameter distribution.

Thermal denaturation studies of amyloid fibrils

Many previous studies have shown that amyloid fibrils are resistant to thermal challenges when compared with the monomeric protein [35,36]. However, to infer if the amyloid fibrils formed from various peptides display similar or different thermal properties, we recorded the variable temperature-circular dichroism (VT-CD) of the solution containing matured fibrils. Reversible thermal changes in the CD ellipticity at 218 nm ($[\theta]_{218}$) corresponding to the β-sheets [28,29,37] were monitored by heating the amyloid fibrils (0.6% w/v) from 20 to 90°C. For P1, the negative maxima $[\theta]_{218}$ increased with increase in temperature, and began to decrease after 70°C and reached a plateau after 85°C. Upon cooling, no clear transition was observed and $[\theta]_{218}$ followed a linear decrease without achieving the original $[\theta]_{218}$ values. Subsequent heating produced traces which followed the $[\theta]_{218}$ values observed during the cooling cycle (Figure 6A). Far UV-CD spectra confirmed a clear transition from β-sheet conformation to a disordered conformation after heating/cooling cycles (Figure 6B). We also monitored the change in intensity of ThT-bound amyloid fibrils with temperature. As shown in Figure 6C, a smooth sigmoidal transition was observed with maximum loss of ThT intensity above 70°C, consistent with the transition observed in the VT-CD experiments. On cooling, no reversible transition was

Biochemical Journal (2017) **474** 1705–1725
DOI: 10.1042/BCJ20170125

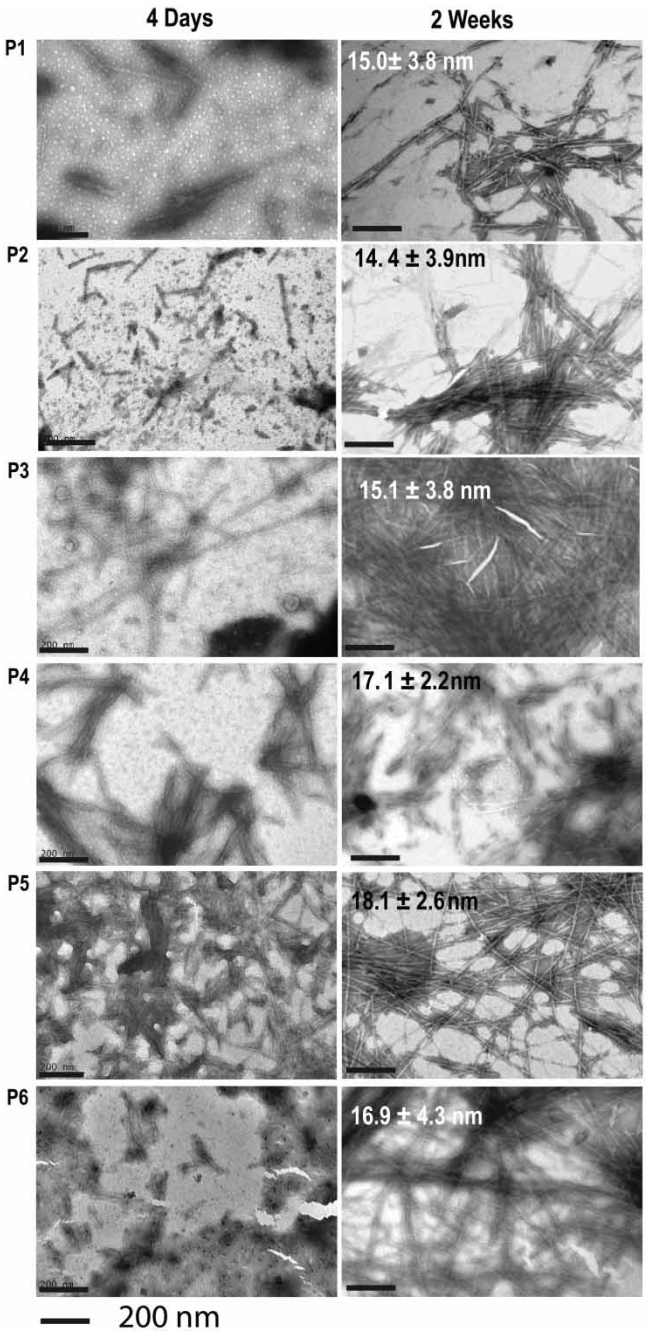

Figure 5. Morphology of amyloid fibrils derived from WT and mutant peptides.

TEM images of the TGFBIp$^{611–633}$WT (P1) and mutant peptides (P2–P6) after 4 days and 2 weeks, acquired with a JEOL JEM-1010 transmission electron microscope using Digital Micrograph™ 1.81.78 for GMS 1.8.0. Stacking densities, distribution and their mean diameters vary between the peptides. It is very clear that the protofibrils of the different mutants display different morphologies, lengths and diameters. While the fibrils are almost fully formed for the P5 peptide, for all the other mutants they are in the process of elongation. Interestingly, the length of the fibrils and the density are in perfect correlation with the aggregation kinetics (Figure 3A–F).

observed, confirming the conversion of amyloid fibrils into monomeric forms (Figure 6C and inset). Similar changes were observed for the peptides P2, P3 and P6 (Supplementary Figure S3). However, for the peptides P4 and P5, a marked reversibility in the thermal transition was observed. For P4, the initial increase in

Biochemical Journal (2017) **474** 1705–1725
DOI: 10.1042/BCJ20170125

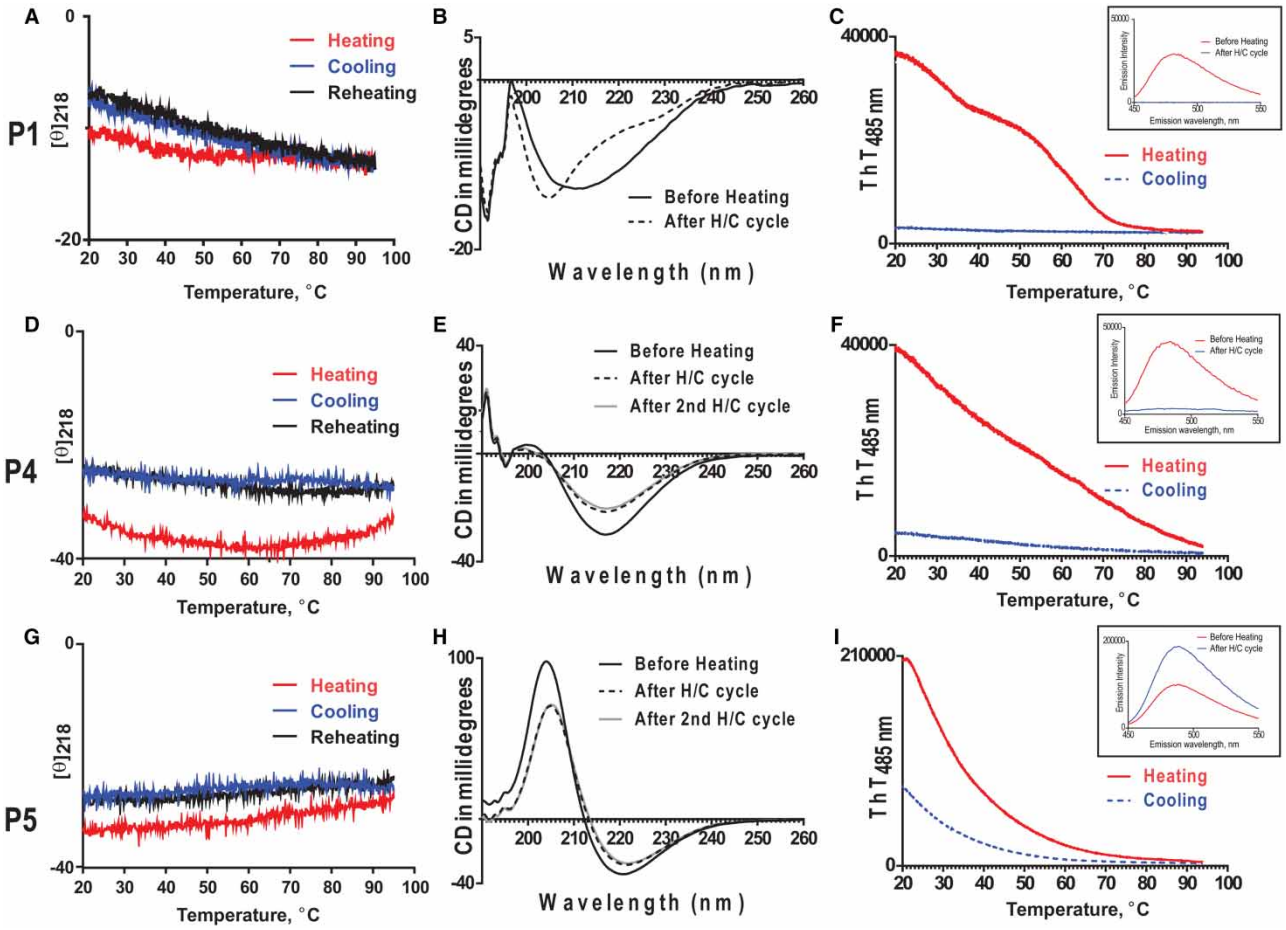

Figure 6. Thermal denaturation studies of amyloid fibrils P1, P4 and P5 using CD spectropolarimetry.

Reversible thermal changes in the CD ellipticity at 218 nm ($[\theta]_{218}$) were monitored by heating the amyloid fibrils from 20 to 90°C (Figure 5A,D,G). Far UV-CD spectra of P1, P4 and P5 peptide fibrils (Figure 5B,E,5H) before heating and after the heating/cooling cycle were measured to study the change in secondary structure. While P1 shows almost no fibrils after heating, P4 and P5 clearly show the presence of β-sheet fibrils. Thermal denaturation using ThT fluorescence studies for P1, P4 and P5 peptides (Figure 5C,F,I) and inset showing both P4 and P5 peptides to be more thermally stable compared with the P1 peptide.

temperature increased the $[\theta]_{218}$ intensity, and at elevated temperature the $[\theta]_{218}$ intensity decreased considerably (Figure 6D). On cooling, the values remained identical and reheating did not alter the $[\theta]_{218}$ intensity values. CD spectra indicated that the β-sheet structure remained intact even after the heating/cooling cycle, although a slight decrease in the amplitude of the negative maximum ∼218 nm was observed (Figure 6E). After second heating/cooling cycle, no obvious change in the secondary structure was observed and the peptide remained intact in β-amyloid conformations. The ThT assay indicated a similar sigmoidal transition upon heating P4 and partial retention of the intensity upon cooling (∼12% of the original ThT intensity; Figures 6F and inset).

The amyloid fibrils prepared from P5 displayed even more remarkable thermal reversibility as shown by the absence of any clear transition upon heating (Figure 6G), although a slight decrease in the CD intensity was observed upon cooling. Reheating did not change the $[\theta]_{218}$ intensity and it remained similar to the values obtained during the cooling cycle over the entire temperature range. CD spectra confirmed the presence of a β-amyloid structure that remained intact even after two heating/cooling cycles, suggesting significant stability of the fibrils compared with the amyloid fibrils derived from other peptides (Figure 6H). The P5 fibril was examined further by performing heating and cooling of the fibrils for five cycles (Supplementary Figure S4). Reheating in the subsequent cycles did not show any changes in intensities. Thermal denaturation using ThT

Biochemical Journal (2017) **474** 1705–1725
DOI: 10.1042/BCJ20170125

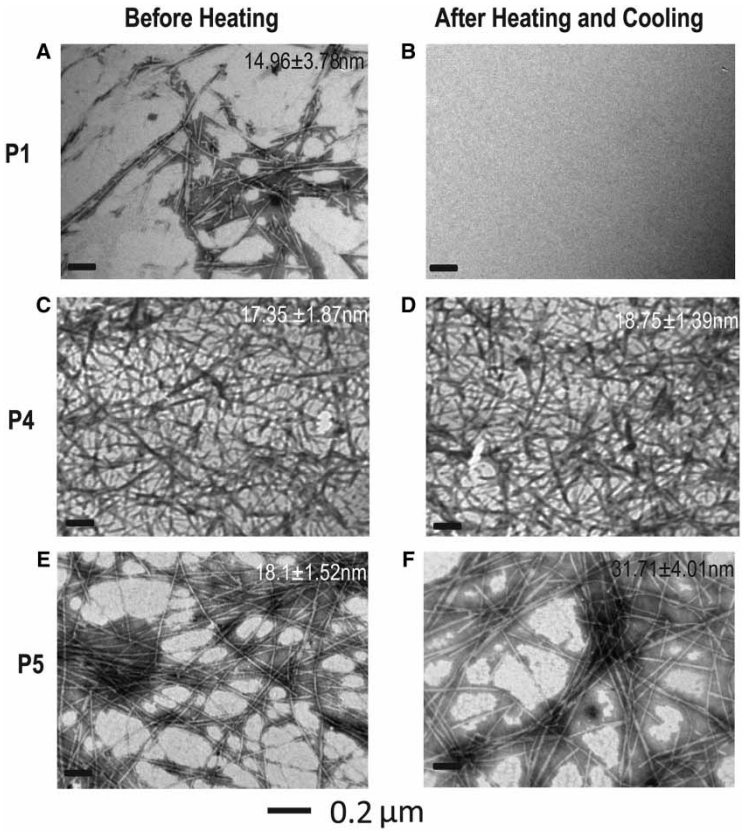

Figure 7. TEM images of the peptide fibrils of P1, P4 and P5 TGFBIp mutants before heating, after heating to 90°C and after cooling to 20°C were acquired. There were no fibrils found on the grid for the P1 peptide after heating. Clear fibrils with almost no difference in their stacking densities were observed for both P4 and P5 peptide fibrils.

fluorescence studies indicated a sharper decrease in the ThT intensity upon heating, and moderate recovery (>50%) was observed upon cooling (Figure 6I and inset) the amyloid fibrils.

TEM was used to further confirm the thermal stability of the amyloid assemblies derived from P1, P4 and P5. For P1, after the thermal denaturation cycle, no amyloid fibrils could be detected, confirming complete disassembly of the fibrils (Figure 7A,B). However, for both P4 and P5, the amyloid structure remained intact (Figure 7C–F). For P5, many fibrils coalesced along the entire length that resulted in a 2-fold increase in the average diameter (18.1 ± 1.52 to 31.71 ± 4.01 nm) of the fibrils. For P4, though the fibrils remained intact, there was little or no coalescence observed and the mean fibrillar diameter remained unaltered (17.5 ± 1.9 nm before heating to 18.8 ± 1.4 nm). These results confirmed the stability achieved by the amyloid fibrils formed from P5 and corroborate the results observed in the VT-CD studies and the ThT assay. Together, these results suggest the possible position-sensitive influence of electrostatic interactions on thermal stability of the amyloid fibrils.

To examine if the thermal ramping rates of heating had any effects on the fibrils formed, we also studied the thermal denaturation of P5 by heating the fibrils to 90°C at various heating rates (0.5, 1 and 2°C/min). In all experiments, the β-sheet structure corresponding to the fibrils remained intact without an apparent change in the temperature at the midpoint, T_m (Supplementary Figure S5).

Since the cationic residue substitution (Gly to Arg) in P5 introduced a trypsin proteolytic site which is not present in P1, we determined the proteolytic stability of the amyloid fibrils derived from P5. The P5 fibrils (300 µg) were digested with trypsin (Trypsin:Fibril = 1:25 ratio) for 12 h and examined by LC–MS/MS and TEM. No discernible peak, which corresponds to the proteolytic fragment (E^{611}PVAEPDIMATNVVHVITNVLQ^{633}), could be detected in the LC–MS spectra. TEM images (Supplementary Figure S6) further confirmed no apparent changes in the morphology of the fibrils before and after trypsin digestion, indicating that Arg 623 residue may form the amyloid fibril core in P5.

Biochemical Journal (2017) **474** 1705–1725
DOI: 10.1042/BCJ20170125

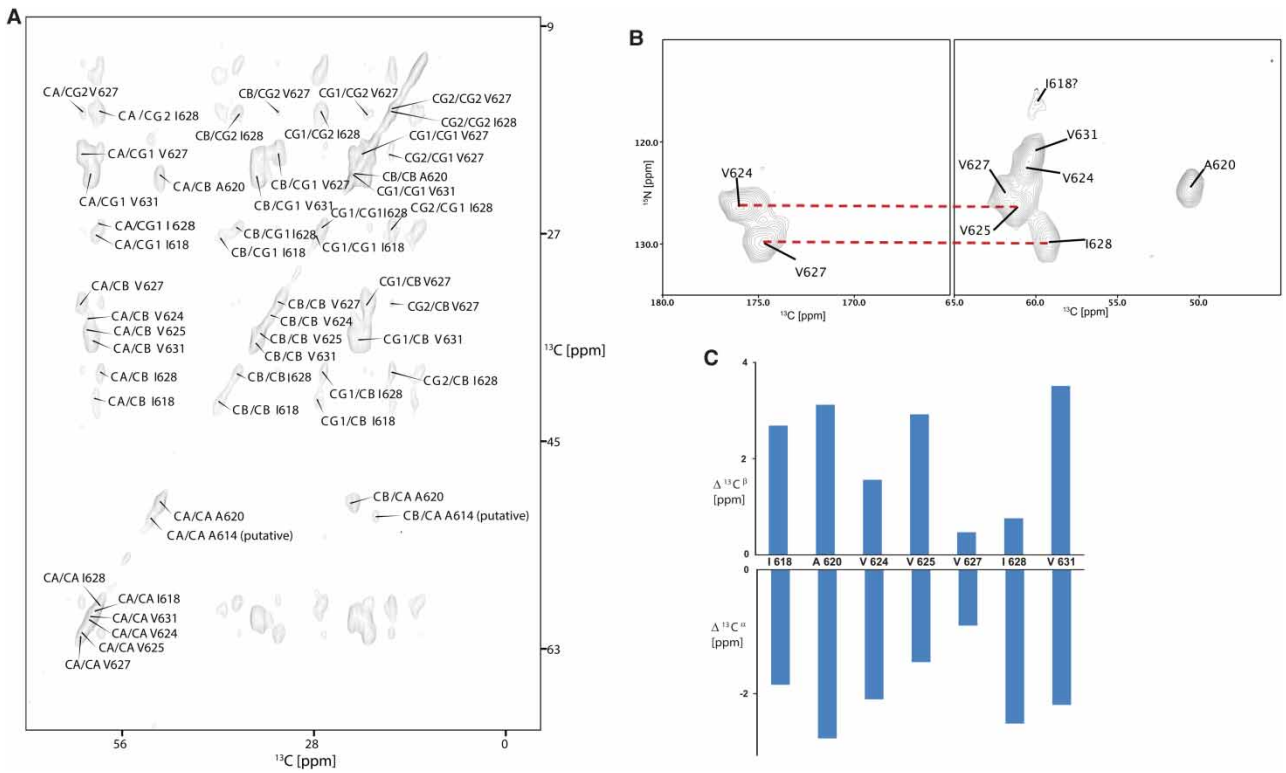

Figure 8. (**A**) Expansion of the aliphatic 2D ^{13}C–^{13}C chemical shift correlation DARR spectra for fibrils derived from the P5 peptide recorded with a 200 ms mixing time. Out of the nine amino acids that were uniformly ^{13}C- and ^{15}N-labeled, peaks were visible for seven amino acids; four valine, two isoleucine and one alanine residues were identified readily based on their characteristic fingerprint region and intra-residue cross-peaks; one valine (V613) and one alanine residue (A614) were not visible for assignment as they might be highly dynamic. (**B**) NCO/NCA plot for peptide P5 used to assign nitrogen chemical shifts. In an NCA experiment, magnetization is transferred from ^{1}H to ^{15}N via cross-polarization and then selectively to the $^{13}C\alpha$ using specific cross-polarization. (**C**) A plot of the C-alpha and C-beta chemical shifts from the rigid part of DARR assignment of the P5 peptide subtracted from the random coil shifts (ΔC^{α} or $\Delta C^{\beta} = [C^{\alpha}$ or C^{β}-$(C^{\alpha}$ or $C^{\beta})_{\text{Random coil shifts}}]$). The plot shows the presence of a β-sheeted secondary structure.

Solid-state NMR for the amyloid fibrils

1D and 2D solid-state NMR was used to study the structure of amyloid fibrils. ^{13}C CP-MAS spectra were recorded to check the quality of the fibrils and structural homogeneity of the samples (Supplementary Figure S7). The ^{13}C cross-polarization spectra indicated that the fibrils formed were uniform and with the resolved ^{13}C resonances and line width smaller than 100 Hz, which warranted further studies using the 2D solid-state experiments.

Among all peptides, the P5 peptide had greater propensity to form amyloid fibrils and the fibrils displayed excellent thermal stability, hence we investigated the possible structural differences in the amyloid fibrils formed from P5 and P1 by solid-state NMR. The DARR [38,39] experiment with a short mixing time was used to identify all intra-residue and 2 bond carbon–carbon correlations. Additionally, 2D NCA and NCO spectra were recorded to aid in the DARR assignment. Figure 8B shows the NCA spectrum of peptide P5 where the ^{1}H magnetization is transferred to ^{15}N via cross-polarization and then selectively to the $^{13}C\alpha$ using band-specific cross-polarization [40]. First, assignments of pairs of sequential residues that are labeled with isotope, VA, GV, VV and VI, were made. The assignments were compared with NCO and NCA spectra, and two pairs of sequential residues with identical chemical shift of 15N were identified. The chemical shift of the side chain from the DARR spectrum was used in the assignment of VV and VI residue pairs. Rest of the signals on NCA was assigned using NCA and DARR spectra. The DARR experiment with the longer mixing time was used for inter-residue connectivity. Out of the nine amino acids that were ^{13}C-labeled for P5, cross-peaks were visible only for seven amino acids (Figure 8A). Out of the two alanine, five valine and two isoleucine residues that

Biochemical Journal (2017) **474** 1705–1725
DOI: 10.1042/BCJ20170125

were uniformly ^{13}C-labeled, one valine (V613) and one alanine residue (A614) were not visible, presumably due to the high intramolecular mobility. The other four valine, two isoleucine and one alanine residues were readily identified based on their characteristic fingerprint chemical shifts and intra-residue cross-peaks.

A plot of the C-α and C-β chemical shifts [41,42] from the rigid part of DARR assignment of the P5 peptide subtracted from the random coil shifts showed a clear β-sheet secondary structure (Figure 8C). The DARR experiment with longer mixing time did not give many extra cross-peaks and the inter-residue connectivities were not observed except between residues V627 and I628, suggesting that the amyloid fibrils may be in a parallel β-sheet arrangement. Thus, solid-state nuclear magnetic resonance (ssNMR) results for the P5 peptide were in agreement with the CD experiments, suggesting that the peptide formed clear β-sheet amyloid fibrils with a parallel β-sheet arrangement. However, for P1, the NCA experiment showed multiple sets of cross-peaks (suggesting the presence of polymorphs) with various confirmations of the amino acids (Supplementary Figure S8A,SB), and hence it was difficult to exhaustively assign the DARR peaks [38–40]. It is likely that the glycine residue in P1 may allow the formation of dynamic β-structured assembly, whereas the presence of arginine in P5 might have stabilized the fibrils through electrostatic interactions, thus producing a homogeneous assembly.

Cytotoxicity of amyloid fibrils on HCSF cells

CD, ThT fluorescence and NMR studies indicated a gradual transition from predominantly unordered confirmations to a β-structured fibrillar assembly with time for all the peptides (except P4 and P5). Figure 9 compared the effect of various freshly prepared peptide solutions and amyloid fibrils on the cell index values derived from xCELLigence. While none of the peptides/amyloid fibrils were cytotoxic to the HCSFs, a significant decrease in the proliferation rate was observed, depending on the nature of the amino acid modifications. For the peptide P1, there was no change in the proliferation rate and the cell index value observed was

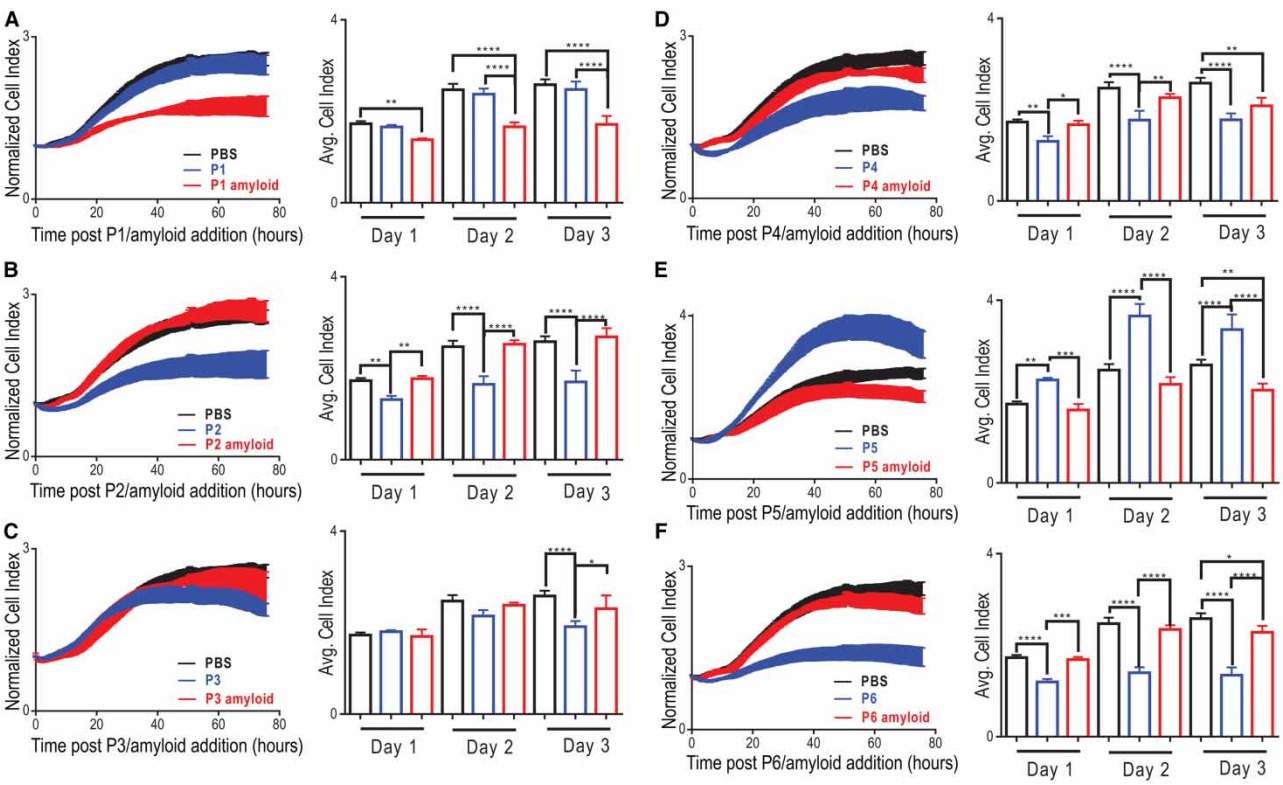

Figure 9. The cell survival following the treatment of the peptides and peptide fibrils of TGFBIp against HCSF cells monitored for 48 h.
HCSF cells seeded at 7000 cells per well on an E-plate 96, in fibroblast media with 5% FBS, were treated with the peptides and peptide fibrils of TGFBIp. Culture was maintained for 48 h in the xCelligence RTCA SP Station, placed in an incubator at 37°C with 5% CO_2. Cell index generated was taken for further analysis.

Biochemical Journal (2017) **474** 1705–1725
DOI: 10.1042/BCJ20170125

comparable with the control (PBS) values. However, P1 amyloid fibers showed a significant inhibitory activity after 24 h incubation ($P \leq 0.05$). The inhibitory effect was more pronounced at 48 and 72 h in the fibrillar state ($P < 0.0001$) compared with control. Amyloid fibrils derived from peptides P4 ($P \leq 0.01$) and P3/P6 ($P \leq 0.05$) displayed significant inhibitory effect compared with the control only after prolonged incubation times (~72 h). Interestingly, the prefibrillar forms of peptides (except P1 and P6) showed more noticeable inhibitory effect on fibroblasts compared with the insoluble amyloid fibrils. For the peptides P2, P4 and P6, the inhibitory effect was visible just after the addition, whereas for P3 the inhibitory effect was significant ($P \leq 0.05$) only after 72 h. The soluble form of P6, which displayed the weakest aggregation kinetics, displayed the maximum inhibitory effect on HCSFs. Interestingly, the soluble form of P5 enhanced the fibroblast proliferation significantly compared with control as well as the insoluble amyloid fibrils. It is interesting to note that P5 has been shown to form fibrils more rapidly compared with the other peptides within 72 h, and it is likely that peptide may have already formed protofibrils during measurements. Together, these results highlight that the soluble and insoluble forms of peptide assemblies display variable interactions with the proliferating fibroblasts.

Discussion

In the normal cornea, the full-length TGFβIp is processed into many shorter fragments by serine proteases [10,16]. The C-terminal truncated isoforms of TGFβIp are the most abundant in the cornea. Other fragments have molecular mass ranging from 29 to 64 kDa. Mutations in amino acid 124, which is located at the 1st FAS-1 domain, lead to a 1.5–3-fold increase in the level of full-length mutant protein in the affected cornea. In addition, R124C generates abnormal accumulation of many proteolytic products in the dystrophic cornea, which are absent from the control populations [10]. Thus, our first objective was to identify tryptic peptide fragments that were enriched in the amyloid fibrils isolated from dystrophic patients relative to normal control.

Spectral counts of the tryptic peptides derived from corneal deposits of three lattice dystrophy patients (two patients with a H626R mutation and one patient with a R124C mutation) showed enrichment of several peptides in the 4th FAS-1 domain that were either absent from control cornea or present in lower abundance. A 32-residue peptide (E^{611}PVAEPDIMATNGVVHVITNVLQPPANRPQER^{642}) was one of the most abundant peptide in the corneal deposits, indicating that this region could form the core of the amyloid fibrils. Mass spectrometric analysis of amyloid fibrils isolated from other dystrophic mutants also showed higher abundance of E^{611}–R^{642} in the semi-tryptic fragments, suggesting the possible pathological association of this fragment in corneal dystrophies [15].

Interestingly, the majority of the amino acid alterations in this region affects the overall net charge of the protein (Supplementary Table S1). A significant number of mutations along this peptide region are associated with clinically relevant phenotypes that result in lattice corneal dystrophy. Since the amyloid-forming properties of any native or mutant peptides derived from this region have not been characterized before, we determined the aggregation properties of a 23-residue peptide (E^{611}PVAEPDIMATNGVVHVITNVLQ^{633}) encompassing this region (E^{611}PVAEPDIMATNGVVHVITNVLQPPANRPQER^{642}) and clinically relevant amino acid alterations (M619K, N622K, N622H, G623R and H626R) which decreased the overall net charge. It is likely that the accumulation of clinically relevant mutant peptides in this region could potentially act as amyloid fibril seeds, triggering the amyloid deposition in the affected patients. In support of this argument, bioinformatic analysis predicted that this region of TGFBIp has significant amyloidogenic potential as well. Therefore, we investigated the amyloidogenic potential, thermal stability and structure of the amyloid fibrils and their interaction with HCSF cells.

Formation of amyloid fibrils from native proteins is an intrinsic characteristic of the constituent amino acid sequence. Consistent with the prediction algorithms, we were able to show that the WT peptide (P1) clearly formed well-defined amyloid fibrils even in the absence of any external additives or other harsh biophysical conditions, e.g. sonication or organic solvents, demonstrating intrinsic amyloidogenic potential of the peptide.

The effect of substitution of positively charged residues had significant effects on the secondary structures and the rate of amyloid formation. It was clear that substitution of residues that possess a low intrinsic β-sheet propensity with residues that have higher propensity to form β-sheets caused a substantial increase in the rate of amyloid formation. This effect was clearly evident for P5 where substitution of glycine by arginine caused a considerable increase in the β-sheet propensity and a higher rate of amyloid formation. Glycine residue lacks side chains and thus confers higher conformational flexibility and low β-sheet propensity, whereas arginine residue could easily be accommodated in a β-sheet structure owing to its ability to form salt bridges with other negatively charged amino acid residues [43]. These results suggest that localized perturbation of the secondary

Biochemical Journal (2017) 474 1705–1725
DOI: 10.1042/BCJ20170125

structure together with a decrease in the overall net charge and the nature of amino acid substitution would possibly accelerate the amyloid fibril formation.

TEM studies indicated that all the peptides formed unbranched amyloid assemblies with increase in incubation time. Morphologically, no apparent changes in the fibrillar assemblies were observed among the fibrils derived from various peptides. However, significant changes in the thermal denaturation profiles were observed as peptides P4 and P5 displayed reversible thermal stability. Their fibrillar structures remained intact and retained the β-sheet structures even after five heating/cooling cycles. The amyloid fibrils formed by other peptides dissociated irreversibly to the disordered monomeric forms. Morel et al. [35] showed that the amyloid fibrils formed by an N47A mutant of the α-spectrin SH3 domain dissociated upon heating to 90°C and reassociated with identical morphology when cooled to ∼65°C. In our study, there was no dissociation of the fibrils or hysteresis observed for P5. Furthermore, we have shown that the thermal denaturation was not affected by the rate of heating, suggesting that the process is not kinetically controlled and appears to occur under equilibrium, confirming remarkable stability achieved by the amyloid fibrils from P5. It is likely that the presence of a multidentate guanidine side chain of the arginine residue could enhance the stability of the fibrils through hydrogen bonding and electrostatic interactions [44].

Solid-state NMR of the amyloid assembly formed by P5 gave insights into the secondary structure of the amyloid fibril formation. Since all the amino acids were not ^{13}C- and ^{15}N-labeled, a complete structure of the peptide could not be determined. Nevertheless, the results suggested that the P5 peptide formed stable and homogenous amyloid fibrils as indicated by the spread of DARR signals when compared with WT peptide. The secondary structures elucidated from the chemical shifts index were in agreement with the other biophysical experiments. However, the DARR spectrum of P1 appeared complex, less-resolved and heterogeneous, presumably due to population of other secondary structures or polymorphisms; therefore, we could not assign the spectra for secondary structure determination of the peptide. The above observations further support the excellent thermal stability of the amyloid fibrils derived from P5, whereas fibrils derived from P1 dissociated completely after heating.

Mutants associated with corneal dystrophies exhibit tissue damage in disease conditions. We have shown previously [27] that β-oligomeric aggregates of TGFBIp mutants display cytotoxicity in HCSF cells. Analysis of the cytotoxicity of peptides on corneal fibroblasts by label-free xCELLigence in both the amyloidogenic and the prefibrillar forms indicated considerable differences in the inhibition of cell proliferation between the two states, although no cytotoxic effect was observed. Interestingly, amyloid fibrils formed by mutant peptides displayed an identical increase in proliferation rates when compared with PBS, whereas amyloid fibrils from native peptide P1 showed a strong inhibitory effect on the proliferation rates. However, in the prefibrillar forms, all the mutant peptides displayed inhibition of cell proliferation when compared with the native P1 peptide, indicating that the oligomers of P1 did not affect the cell proliferation. Among the mutant peptides in their prefibrillar form, P6 displayed the strongest inhibitory effect. The identification of peptide fragments around the amino acid sequence of P6 and accumulation of oligomers in patients with the H626R phenotype could be responsible for the lesions observed in them.

The formation of amyloid fibrils and the phenotype of the disease depend on two main factors [45], the position of the mutation and the type of amino acid change compared with the native form. While the critical length of peptides/proteins that constitute amyloid deposits in dystrophic patients remains unknown, our results suggest that subtle decrease in the overall net charge, nature of amino acid substitution and the ability to form β-sheet structure could confer enhanced propensity to form amyloid aggregates or may accelerate the fibrillation of TGFBIp proteins/peptides.

Previous reports from Enghild and colleagues identified the presence of smaller peptide fragments of the protein accumulating in the cornea possibly due to aberrant proteolytic processing [15,16,18]. In particular, an increased abundance of peptide fragment L^{128}–R^{172} in patients' cornea carrying the R124C mutation was reported. Schmitt-Bernard et al. [46] studied the amyloidogenicity of a 22 amino acid-long L110-Q131 peptide which partly overlaps with the L128–R172 peptide fragment and showed that the mutant peptides accelerated the amyloid fibrillation in comparison with native peptides. Together with their studies, our studies shed light into the importance of investigating the amyloid propensity of pathologically relevant peptide fragments.

Conclusion

Using mass spectrometry, we identified a short peptide fragment in the 4th FAS-1 domain that was enriched in the amyloid deposits of the dystrophic patients with H626R and R124C mutations. The amyloid propensity of

this fragment along with five other clinically relevant substitutions, which decreased the overall net charge, was investigated by various biophysical studies. We showed that a decrease in the overall net charge of the peptide altered the secondary structure and accelerated the amyloid formation, depending on the nature of cationic residues and position of the substitution. In terms of morphology, the matured amyloid fibrils formed by the various peptides were indistinguishable, although considerable differences were observed in the thermal denaturation scans and ssNMR structure. The latter revealed the intact population β-structured assembly in P5, whereas amyloid fibrils from P1 populate a heterogeneous population of conformers. Consistent with these observations, amyloid fibrils formed by P5 displayed remarkable thermal stability, whereas P1 amyloid fibrils readily transformed into the monomeric form. The increased thermal stability suggests that the reversal or dissolution of the fibrils could be difficult and future therapeutic interventions must take into consideration this aspect. The peptides derived from our studies may also provide a useful model for investigating the effects of pharmacological agents on dissociation of amyloid fibrils since the experiments were conducted under physiological conditions.

Abbreviations

1D, one-dimensional; 2D, two-dimensional; ACN, acetonitrile; AUC, area under the curve; CD, circular dichroism; CP-MAS, cross-polarization magic-angle spinning; DARR, dipolar-assisted rotational resonance; DSS, 4,4-dimethyl-4-silapentane-1-sulfonic acid; emPAI, exponentially modified protein abundance index; FA, formic acid; FAS-1, fasciclin-like domain-1; HCSF, cultured human corneal fibroblast; LCD, lattice corneal dystrophy; LCM, laser capture microdissection; LC-MS, liquid chromatography-mass spectrometry; MRW, mean residual weight; PBS, phosphate-buffered saline; RTCA, real-time cell analysis; ssNMR, solid-state nuclear magnetic resonance; TD, time domain; TEM, transmission electron microscopy; *TGFBI*, transforming growth factor beta-induced; TGFBIp, transforming growth factor beta-induced protein; ThT, Thioflavin T; VT-CD, variable temperature-circular dichroism; WT, wild type.

Author Contribution

K.P., R.L. and J.S.M. designed the experiments. V.A., E.M., E.G.T.L. and L.W.T. performed experiments. V.A. and E.M. analyzed data. T.Y. and T.N. recorded ss-NMR experiments. B.L.G., G.S.L.P. and S.S.C. performed cytotoxicity assays. V.A., E.M., K.P., R.L. and J.S.M. wrote the manuscript.

Acknowledgements

The authors acknowledge the funding support from National Medical Research Council Singapore [Clinician Scientist-Individual Research Grant R978/87/2012, Singapore National Eye Centre-Health Research Endowment Fund R1071/91/2013 and Singapore National Eye Centre-Health Research Endowment Fund R1209/15/2015].

Competing Interests

The Authors declare that there are no competing interests associated with the manuscript.

References

1 Munier, F.L., Korvatska, E., Djemaï, A., Paslier, D.L., Zografos, L., Pescia, G. et al. (1997) Kerato-epithilin mutations in four 5q-31 linked corneal dystrophies. *Nat. Genet.* **15**, 247–251 doi:10.1038/ng0397-247
2 Kannabiran, C. and Klintworth, G.K. (2006) TGFBI gene mutations in corneal dystrophies. *Hum. Mutat.* **27**, 615–625 doi:10.1002/humu.20334
3 Klintworth, G.K. (2009) Corneal dystrophies. *Orphanet J. Rare Dis.* **4**, 7 doi:10.1186/1750-1172-4-7
4 Lakshminarayanan, R., Chaurasia, S.S., Anandalakshmi, V., Chai, S.-M., Murugan, E., Vithana, E.N. et al. (2014) Clinical and genetic aspects of the TGFBI-associated corneal dystrophies. *Ocul. Surf.* **12**, 234–251 doi:10.1016/j.jtos.2013.12.002
5 El Kochairi, I., Letovanec, I., Uffer, S., Munier, F.L., Chaubert, P. and Schorderet, D.F. (2006) Systemic investigation of keratoepithelin deposits in TGFBI/BIGH3-related corneal dystrophy. *Mol. Vis.* **12**, 461–466 PMID:16710170
6 Runager, K., Enghild, J.J. and Klintworth, G.K. (2008) Focus on molecules: transforming growth factor beta induced protein (TGFBIp). *Exp. Eye Res.* **87**, 298–299 doi:10.1016/j.exer.2007.12.001
7 Skonier, J., Neubauer, M., Madisen, L., Bennett, K., Plowman, G.D. and Purchio, A.F. (1992) cDNA cloning and sequence analysis of βig-h3, a novel gene induced in a human adenocarcinoma cell line after treatment with transforming growth factor-β. *DNA Cell Biol.* **11**, 511–522 doi:10.1089/dna.1992.11.511
8 Bae, J.-S., Lee, S.-H., Kim, J.-E., Choi, J.-Y., Park, R.-W., Yong Park, J. et al. (2002) βig-h3 supports keratinocyte adhesion, migration, and proliferation through α3β1 integrin. *Biochem. Biophys. Res. Commun.* **294**, 940–948 doi:10.1016/S0006-291X(02)00576-4
9 Kim, J.-E., Kim, S.-J., Lee, B.-H., Park, R.-W., Kim, K.-S. and Kim, I.-S. (2000) Identification of motifs for cell adhesion within the repeated domains of transforming growth factor-β-induced gene, βig-h3. *J. Biol. Chem.* **275**, 30907–30915 doi:10.1074/jbc.M002752200

Biochemical Journal (2017) **474** 1705–1725
DOI: 10.1042/BCJ20170125

10 Korvatska, E., Henry, H., Mashima, Y., Yamada, M., Bachmann, C., Munier, F.L. et al. (2000) Amyloid and non-amyloid forms of 5q31-linked corneal dystrophy resulting from kerato-epithelin mutations at Arg-124 are associated with abnormal turnover of the protein. *J. Biol. Chem.* **275**, 11465–11469 doi:10.1074/jbc.275.15.11465
11 Schmitt-Bernard, C.-F., Chavanieu, A., Herrada, G., Subra, G., Arnaud, B., Demaille, J.G. et al. (2002) BIGH3 (TGFBI) Arg124 mutations influence the amyloid conversion of related peptides *in vitro*. *Eur. J. Biochem.* **269**, 5149–5156 doi:10.1046/j.1432-1033.2002.03205.x
12 Clout, N.J., Tisi, D. and Hohenester, E. (2003) Novel fold revealed by the structure of a FAS1 domain pair from the insect cell adhesion molecule fasciclin I. *Structure* **11**, 197–203 doi:10.1016/S0969-2126(03)00002-9
13 Suesskind, D., Auw-Haedrich, C., Schorderet, D.F., Munier, F.L. and Loeffler, K.U. (2006) Keratoepithelin in secondary corneal amyloidosis. *Graefes Arch. Klin. Exp. Ophthalmol.* **244**, 725–731 doi:10.1007/s00417-005-0153-x
14 Tan, Z., Shang, S. and Danishefsky, S.J. (2011) Rational development of a strategy for modifying the aggregatibility of proteins. *Proc. Natl Acad. Sci. U. S.A.* **108**, 4297–4302 doi:10.1073/pnas.1100195108
15 Courtney, D.G., Toftgaard Poulsen, E., Kennedy, S., Moore, J.E., Atkinson, S.D., Maurizi, E. et al. (2015) Protein composition of TGFBI-R124C- and TGFBI-R555W-associated aggregates suggests multiple mechanisms leading to lattice and granular corneal dystrophy. *Investig. Opthalmol. Vis. Sci.* **56**, 4653 doi:10.1167/iovs.15-16922
16 Karring, H., Poulsen, E.T., Runager, K., Thogersen, I.B., Klintworth, G.K., Hojrup, P. et al. (2013) Serine protease HtrA1 accumulates in corneal transforming growth factor beta induced protein (TGFBIp) amyloid deposits. *Mol. Vis.* **19**, 861–876 PMID:23592924
17 Karring, H., Runager, K., Thøgersen, I.B., Klintworth, G.K., Højrup, P. and Enghild, J.J. (2012) Composition and proteolytic processing of corneal deposits associated with mutations in the TGFBI gene. *Exp. Eye Res.* **96**, 163–170 doi:10.1016/j.exer.2011.11.014
18 Sørensen, C.S., Runager, K., Scavenius, C., Jensen, M.M., Nielsen, N.S., Christiansen, G. et al. (2015) Fibril core of transforming growth factor beta-induced protein (TGFBIp) facilitates aggregation of corneal TGFBIp. *Biochemistry* **54**, 2943–2956 doi:10.1021/acs.biochem.5b00292
19 Yuan, C., Berscheit, H.L. and Huang, A.J.W. (2007) Identification of an amyloidogenic region on keratoepithelin via synthetic peptides. *FEBS Lett.* **581**, 241–247 doi:10.1016/j.febslet.2006.12.019
20 Lakshminarayanan, R., Vithana, E.N., Chai, S.-M., Chaurasia, S.S., Saraswathi, P., Venkatraman, A. et al. (2011) A novel mutation in transforming growth factor-beta induced protein (TGFβIp) reveals secondary structure perturbation in lattice corneal dystrophy. *Br. J. Ophthalmol.* **95**, 1457–1462 doi:10.1136/bjophthalmol-2011-300651
21 Aldave, A.J., Yellore, V.S., Sonmez, B., Bourla, N., Salem, A.K., Khan, M.A. et al. (2008) A novel variant of combined granular-lattice corneal dystrophy associated with the Met619Lys mutation in the TGFBI gene. *Arch. Ophthalmol.* **126**, 371–377 doi:10.1001/archopht.126.3.371
22 Stewart, H., Black, G.C.M., Donnai, D., Bonshek, R.E., McCarthy, J., Morgan, S. et al. (1999) A mutation within exon 14 of the TGFBI (BIGH3) gene on chromosome 5q31 causes an asymmetric, late-onset form of lattice corneal dystrophy. *Ophthalmology* **106**, 964–970 doi:10.1016/S0161-6420(99)00539-4
23 Munier, F.L., Frueh, B.E., Othenin-Girard, P., Uffer, S., Cousin, P., Wang, M.X. et al. (2002) BIGH3 mutation spectrum in corneal dystrophies. *Invest. Ophthalmol. Vis. Sci.* **43**, 949–954 PMID:11923233
24 Gruenauer-Kloevekorn, C., Clausen, I., Weidle, E., Wolter-Roessler, M., Tost, F., Völcker, H.E. et al. (2009) TGFBI (BIGH3) gene mutations in German families: two novel mutations associated with unique clinical and histopathological findings. *Br. J. Ophthalmol.* **93**, 932–937 doi:10.1136/bjo.2008.142927
25 Yang, J., Han, X., Huang, D., Yu, L., Zhu, Y., Tong, Y. et al. (2010) Analysis of *TGFBI* gene mutations in Chinese patients with corneal dystrophies and review of the literature. *Mol. Vis.* **16**, 1186–1193 PMC:2901189
26 Murugan, E., Venkataraman, A., Beuerman, R.W., Lakshminarayanan, R. and Mehta, J.S. (2015) TGFβIP model peptides with mutations reducing the overall charge forms cytotoxic amyloid fibrils. *Invest. Ophthalmol. Vis. Sci.* **56**, 3079
27 Murugan, E., Venkatraman, A., Lei, Z., Mouvet, V., Rui Yi Lim, R., Muruganantham, N. et al. (2016) pH induced conformational transitions in the transforming growth factor β-induced protein (TGFβIp) associated corneal dystrophy mutants. *Sci. Rep.* **6**, 23836 doi:10.1038/srep23836
28 Dobson, C.M. (2003) Protein folding and misfolding. *Nature* **426**, 884–890 doi:10.1038/nature02261
29 Chiti, F. and Dobson, C.M. (2006) Protein misfolding, functional amyloid, and human disease. *Ann. Rev. Biochem.* **75**, 333–366 doi:10.1146/annurev.biochem.75.101304.123901
30 Monsellier, E., Ramazzotti, M., de Laureto, P.P., Tartaglia, G.-G., Taddei, N., Fontana, A. et al. (2007) The distribution of residues in a polypeptide sequence is a determinant of aggregation optimized by evolution. *Biophys. J.* **93**, 4382–4391 doi:10.1529/biophysj.107.111336
31 Matsumura, S., Uemura, S. and Mihara, H. (2004) Fabrication of nanofibers with uniform morphology by self-assembly of designed peptides. *Chemistry* **10**, 2789–2794 doi:10.1002/chem.200305735
32 LeVine, H. (1999) *[18] Quantification of β-Sheet Amyloid Fibril Structures with Thioflavin T. Methods in Enzymology*, Elsevier BV, pp. 274–284
33 Biancalana, M. and Koide, S. (2010) Molecular mechanism of Thioflavin-T binding to amyloid fibrils. *Biochim. Biophys. Acta Proteins Proteomics* **1804**, 1405–1412 doi:10.1016/j.bbapap.2010.04.001
34 Groenning, M. (2010) Binding mode of Thioflavin T and other molecular probes in the context of amyloid fibrils — current status. *J. Chem. Biol.* **3**, 1–18 doi:10.1007/s12154-009-0027-5
35 Morel, B., Varela, L. and Conejero-Lara, F. (2010) The thermodynamic stability of amyloid fibrils studied by differential scanning calorimetry. *J. Phys. Chem. B* **114**, 4010–4019 doi:10.1021/jp9102993
36 Sasahara, K., Naiki, H. and Goto, Y. (2005) Kinetically controlled thermal response of β2-microglobulin amyloid fibrils. *J. Mol. Biol.* **352**, 700–711 doi:10.1016/j.jmb.2005.07.033
37 Conchillo-Solé, O., de Groot, N.S., Avilés, F.X., Vendrell, J., Daura, X. and Ventura, S. (2007) AGGRESCAN: a server for the prediction and evaluation of 'hot spots' of aggregation in polypeptides. *BMC Bioinf.* **8**, 65 doi:10.1186/1471-2105-8-65
38 Takegoshi, K., Nakamura, S. and Terao, T. (2003) 13C–1H dipolar-driven 13C–13C recoupling without 13C rf irradiation in nuclear magnetic resonance of rotating solids. *J. Chem. Phys.* **118**, 2325–2341 doi:10.1063/1.1534105
39 Takegoshi, K., Nakamura, S. and Terao, T. (2001) 13C–1H dipolar-assisted rotational resonance in magic-angle spinning NMR. *Chem. Phys. Lett.* **344**, 631–637 doi:10.1016/S0009-2614(01)00791-6

40 Baldus, M., Petkova, A.T., Herzfeld, J. and Griffin, R.G. (1998) Cross polarization in the tilted frame: assignment and spectral simplification in heteronuclear spin systems. *Mol. Phys.* **95**, 1197–1207 doi:10.1080/00268979809483251
41 Spera, S. and Bax, A. (1991) Empirical correlation between protein backbone conformation and C.alpha. and C.beta. 13C nuclear magnetic resonance chemical shifts. *J. Am. Chem. Soc.* **113**, 5490–5492 doi:10.1021/ja00014a071
42 Shen, Y. and Bax, A. (2013) Protein backbone and sidechain torsion angles predicted from NMR chemical shifts using artificial neural networks. *J. Biomol. NMR* **56**, 227–241 doi:10.1007/s10858-013-9741-y
43 Gerling, U.I.M., Brandenburg, E., Berlepsch, H.v., Pagel, K. and Koksch, B. (2011) Structure analysis of an amyloid-forming model peptide by a systematic glycine and proline scan. *Biomacromolecules* **12**, 2988–2996 doi:10.1021/bm200587m
44 Chen, L. and Liang, J.F. (2013) Peptide fibrils with altered stability, activity, and cell selectivity. *Biomacromolecules* **14**, 2326–2331 doi:10.1021/bm400618m
45 Schmitt-Bernard, C.-F., Schneider, C. and Argilés, A. (2002) Clinical, histopathologic, and ultrastructural characteristics of BIGH3(TGFBI) amyloid corneal dystrophies are supportive of the existence of a new type of LCD: the LCDi. *Cornea* **21**, 463–468 doi:10.1097/00003226-200207000-00006
46 Schmitt-Bernard, C.F., Chavanieu, A., Derancourt, J., Arnaud, B., Demaille, J.G., Calas, B. and Argiles, A. (2000) In vitro creation of amyloid fibrils from native and Arg124Cys mutated betaIGH3((110-131)) peptides, and its relevance for lattice corneal amyloid dystrophy type I. *Biochem. Biophys. Res. Commun.* **273**, 649–653